THE JOURNAL OF PHYSICAL CHEMISTRY C

Article

Cite This: J. Phys. Chem. C 2018, 122, 5813−5819

pubs.acs.org/JPCC

Temperature Dependence of the Amplified Spontaneous Emission from $CsPbBr_3$ Nanocrystal Thin Films

Antonio Balena,[†] Andrea Perulli,[†] Manuel Fernandez,[†] Maria Luisa De Giorgi,[†] Georgian Nedelcu,[‡,§] Maksym V. Kovalenko,[‡,§] and Marco Anni*[,†]

[†]Dipartimento di Matematica e Fisica "Ennio De Giorgi", Università del Salento, Via per Arnesano, 73100 Lecce, Italy

[‡]Institute of Inorganic Chemistry, Department of Chemistry and Applied Bioscience, ETH Zürich, CH-8093 Zürich, Switzerland

[§]Laboratory for Thin Films and Photovoltaics, Empa—Swiss Federal Laboratories for Materials Science and Technology, CH-8600 Dübendorf, Switzerland

Supporting Information

ABSTRACT: Cesius lead halide perovskite colloidal nanocrystals are among the most promising perovskite systems for light-emitting devices applications due to their high fluorescence quantum yield and high optical gain at room temperature. In this letter, we report on the first investigation of temperature dependence of amplified spontaneous emission (ASE) properties of thin films of $CsPbBr_3$ nanocrystals. We demonstrate that ASE is strongly temperature-dependent, with a complex variation in temperature of the ASE intensity, threshold, and peak wavelength. The joint investigation of the photoluminescence (PL) spectra below and above the ASE threshold allows us to conclude that the temperature increase results in the formation of disordered subdomains emitting in the low-energy tail of the PL spectra, leading to the existence of three emission regimes with transitions at about 90 and 170 K, with individually different temperature dependences.

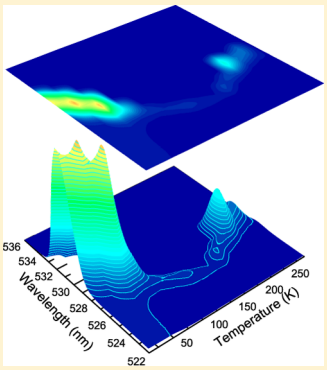

INTRODUCTION

Lead halide perovskite thin films are receiving an increasing attention in the last few years, initially stimulated by the impressive performances improvement of solar cells, recently reaching a record power conversion efficiency of 22.7%.[1] Beyond the excellent photovoltaic properties, allowed by the combination of high absorption cross section, large carrier diffusion length, and low trap density,[2,3] lead halide perovskites also show excellent optical properties, like high photoluminescence quantum yield (PLQY),[4] fully tunable emission from the blue to the near infrared,[4−6] by adjusting the material chemical composition[7,8] and exploiting the quantum confinement in nanostructures, low amplified spontaneous emission (ASE) threshold, and high optical gain at room temperature.[9,10] These properties, together with the possibility of deposition from solution, have been recently exploited for the realization of the first optically pumped perovskite lasers using different cavity geometries, like vertical microcavity lasers,[11] whispering gallery mode lasers,[10] random lasers,[12] and distributed feedback lasers.[13]

The high applicative interest of the solution-processed perovskites thin films also stimulated the research on the basic photophysical processes affecting the material properties. In this frame, the investigation of the optical properties as a function of the temperature, starting from cryogenic temperatures, is a very powerful tool, and it has been to date exploited to investigate the effects of the variation of the exciton−phonon coupling,[14,15] of trapping or detrapping processes,[14,16] of exciton dissociation[15,17] and of crystalline phase variation on the absorption,[18,19] the photoluminescence,[14−17,20−23] and the excitation relaxation dynamics[14,16,17,21−23] of perovskite thin films.

Despite the rich scenario of temperature-induced processes affecting the basic photophysics of perovskite thin films, the ASE temperature dependence investigation is to date limited to few experiments, on polycrystalline bulk thin films of $MAPbI_3$[24,25] and of $CsPbBr_3$,[26] evidencing effects of the crystalline phase transitions and of the exciton trapping and detrapping processes, respectively. On the contrary, the temperature dependence of the ASE of thin films of colloidal perovskite nanocrystals has been to date not investigated yet.

In this paper, we report on the first investigation of the temperature dependence of the amplified spontaneous emission properties of a thin film of $CsPbBr_3$ nanocrystals between 10 and 290 K, excited by a nitrogen laser (3 ns pulses at 337 nm, repetition rate 10 Hz). We demonstrate that the temperature decrease to 10 K results in a considerable increase of the optical gain and a strong decrease of the ASE threshold. A complex temperature dependence of the ASE peak energy, intensity, and threshold is observed, evidencing the presence of three different emissions regimes, namely, below 90 K, between 90 and 170 K, and above 170 K, with individually different temperature

Received: February 9, 2018
Revised: February 19, 2018
Published: February 20, 2018

DOI: 10.1021/acs.jpcc.8b01419
J. Phys. Chem. C 2018, 122, 5813−5819

dependences. The joint investigation of the emission properties above and below the ASE threshold indicates the formation of new emitting species at low energy and at characteristic temperatures of 90 and 170 K, ascribed to partially disordered crystalline subdomains. We demonstrate that the ASE properties of the films are strongly affected by the formation of these domains and are mainly determined by the emission properties of the species emitting at lower energy.

EXPERIMENTAL SECTION

Nanocrystal Synthesis, Thin-Film Deposition and Characterization. The $CsPbBr_3$ nanocrystals have been synthesized by following the report of Protesescu et al.[4] but with some modifications. The detailed procedure is described in the Supporting Information.

The photoluminescence quantum yield (PLQY) has been measured in solution against fluorescein in 0.1 M NaOH (excitation wavelength 488 nm).[27]

The nanocrystals shape and dimensions have been investigated using a Hitachi HT7700 EXALENS microscope operated at 100 kV.

The active film has been deposited by drop-casting onto glass substrates at room temperature and in air. To improve the film morphology, the film was left to dry in a Petri dish, thus slowing the solvent evaporation.

The film morphology has been investigated by a JEOL JSM-6480LV scanning electron microscope (SEM), operated at 10 kV.

The fluorescence maps were measured by a Nikon Eclipse C1 fluorescence inverted microscope (20× DIC Plan-Apochromat objective, 0.50 numerical aperture) by exciting with a spectrally filtered mercury lamp in the range 470−490 nm and collecting the fluorescence in the range 520−560 nm.

PL, Amplified Spontaneous Emission, and Gain Measurements. An LTB MNL 100 nitrogen laser delivering 3 ns pulses at 355 nm, with a peak energy up to 155 μJ, was used as excitation source of the PL, ASE and optical gain measurements. The pump laser has been focused by a cylindrical lens on a rectangular stripe with length up to 4 mm and width of 100 μm. The laser excitation density has been varied by a variable neutral filter. The sample emission was collected from the sample edge after waveguiding along the pumped stripe, spectrally dispersed by a Acton 750 spectrometer, and detected by a Andor Peltier cooled CCD. The spectral resolution was about 0.5 nm. The sample temperature has been changed by a closed-circle He cryostat, allowing to change the temperature in the range of 10−290 K.

RESULTS AND DISCUSSION

As a first step in our experiment, we investigated the excitation density dependence of the PL spectra at room temperature (290 K). The PL spectrum shows, at low excitation density, a single emission resonance peaked at 513.7 nm (2.414 eV) with a full width at half-maximum (FWHM) of 22.8 nm (108 meV, see Figure 1a). As the excitation density increases, a progressive intensity increase is observed with a clear line shape variation due to the appearance of a narrow band peaked at about 526.7 nm, progressively dominating the emission as the excitation density is further increased. These features are comparable to the ones previously reported in similar samples both under femtosecond and nanosecond pumping[10] and are ascribed to ASE. The ASE band appearance results in a clear slope variation

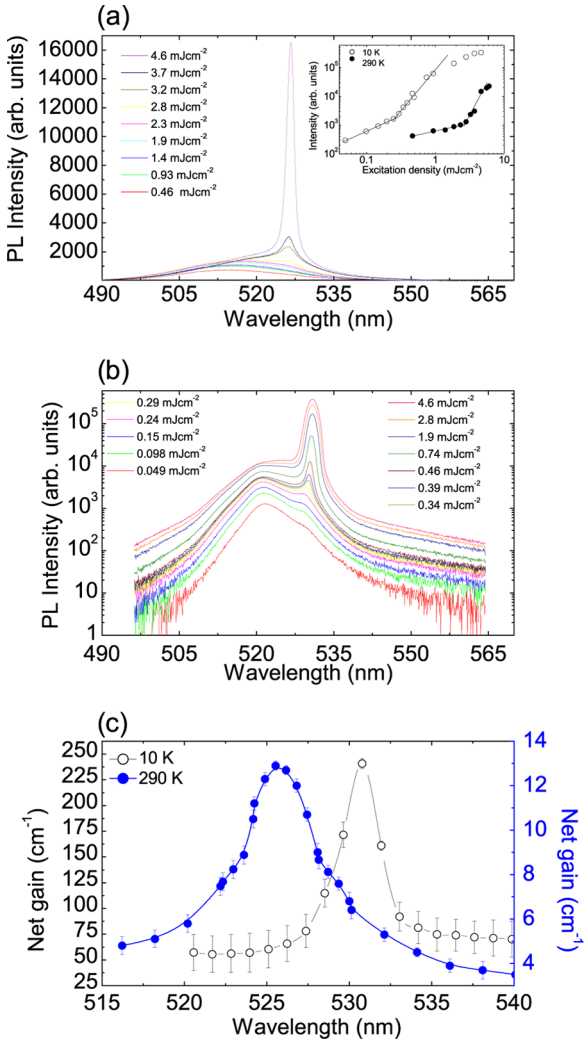

Figure 1. (a) Excitation density dependence of the PL spectra at room temperature (290 K). A clear ASE band is visible at 526.7 nm. Inset: excitation density dependence of the total PL intensity, showing the slope increase across the ASE threshold. (b) Excitation density dependence of the PL spectra at T = 10 K. (c) Net gain spectrum at T = 10 and 290 K.

of the total intensity dependence on the excitation density (see inset of Figure 1a). We estimated an ASE threshold of about 2.55 mJ cm^{-2} by continuously increasing the pump excitation density and determining the minimum excitation density that allows to observe the ASE band appearance in the spectra. The optical gain spectrum, measured with the variable stripe method at an excitation density of 6.0 mJ cm^{-2}, shows a single peak at 525.6 nm with a maximum value of 12.9 cm^{-1} (see Figure 1c).

When the temperature is decreased to 10 K (see Figure 1b), we observe, at low excitation density, a PL peak red shift to 521.5 nm (2.377 eV) and a FWHM reduction to 7.8 nm (35.6 meV). As the excitation density increases, a clear ASE band is observed, peaked at 530.5 nm, with a strongly reduced threshold of 147 μJ cm^{-2}. The temperature reduction also leads to a considerable enhancement of the net optical gain, reaching the remarkable maximum value of 241 cm^{-1} (see Figure 1c) at an excitation density of 930 μJ cm^{-2}. Thus, the temperature decrease to 10 K allows to increase the maximum gain value by about 19 times, at an excitation density 6.5 times

DOI: 10.1021/acs.jpcc.8b01419
J. Phys. Chem. C 2018, 122, 5813−5819

lower, evidencing a considerable enhancement of the gain properties.

To have a clear understanding of the temperature-dependent processes affecting the optical gain in our sample, we thus measured the emission spectra at a common excitation density of 4.6 mJ cm^{-2} (above the room temperature ASE threshold).

The obtained results, reported in Figure 2a as a two-dimensional (2D) map, show a complex temperature dependence, in particular as the temperature increases we observe that:

(1) The ASE peak position shows a progressive linear (in energy) blue shift (see Figure 2b) up to 90 K with a best fit slope of 250 ± 4 μeV K^{-1}, followed by a weaker blue shift up to 170 K with a slope of 67 ± 7 μeV K^{-1}, then a red shift up to 270 K, and finally a blue shift up to 290 K.
(2) The integrated spectrum intensity is almost constant up to 50 K (see Figure 2c), then a strong intensity reduction is observed up to 90 K, followed by a weaker quenching up to 170 K. A strong intensity recovery is observed up to 230 K, finally followed by a further quenching up to 290 K.
(3) The ASE threshold shows a strong initial increase up to 90 K (see Figure 2c), followed by a weaker increase up to 190 K. Then an abrupt decrease is observed between 190 and 210 K, followed by a continuous threshold increase up to 290 K.

Overall, these results evidence the existence of two common temperatures at which the temperature dependences change, namely, 90 K and between 170 and 190 K, suggesting the presence of three different emission regimes.

To rationalize the previous results, we also investigated the PL temperature dependence below the ASE threshold at a common excitation density of 150 μJ cm^{-2}.

The PL spectrum at T = 10 K (see Figure 3a) shows a main narrow peak at 521.5 nm (2.377 eV) with a FWHM of 8.6 nm (39.2 meV).

When the temperature increases, clear variations of the line shape, the PL peak energy, and the PL intensity are observed. In particular, we observe that from T = 10 K to 30 K a strong intensity decrease of the sharp peak dominating the PL at T = 10 K takes place, giving rise to a much broader and featureless spectrum, red-shifted of 1.1 nm (5 meV) (see Figure 3d), and with a FWHM increased to 11.4 nm (51.7 meV). When the temperature is further increased, the following features are observed:

(1) The PL peak energy (see Figure 3b,d) shows a linear blue shift with a best fit slope of 239 ± 13 μeV K^{-1} up to 170 K and a clear slope reduction down to 48 ± 5 μeV K^{-1} at higher temperatures.
(2) The PL intensity (see Figure 3c) initially shows a very strong intensity decrease between 10 and 90 K (about 95% intensity reduction), followed by a much weaker intensity decrease up to 170 K, and then by a very clear recovery (7 times) up to 290 K.

The linear blue shift of the PL peak energy has been already demonstrated in many perovskite materials,[14,16,17,20,21,25] evidencing a different behavior with respect to typical inorganic semiconductors, whose PL peak energy typically decreases as the temperature increases.[28] This behavior evidences that in these materials the blue shift induced by thermal expansion[29] dominates over the band gap renormalization due to the increase of the interaction with phonons (leading to a red shift).[30] The best fit value of the peak energy blue shift up to

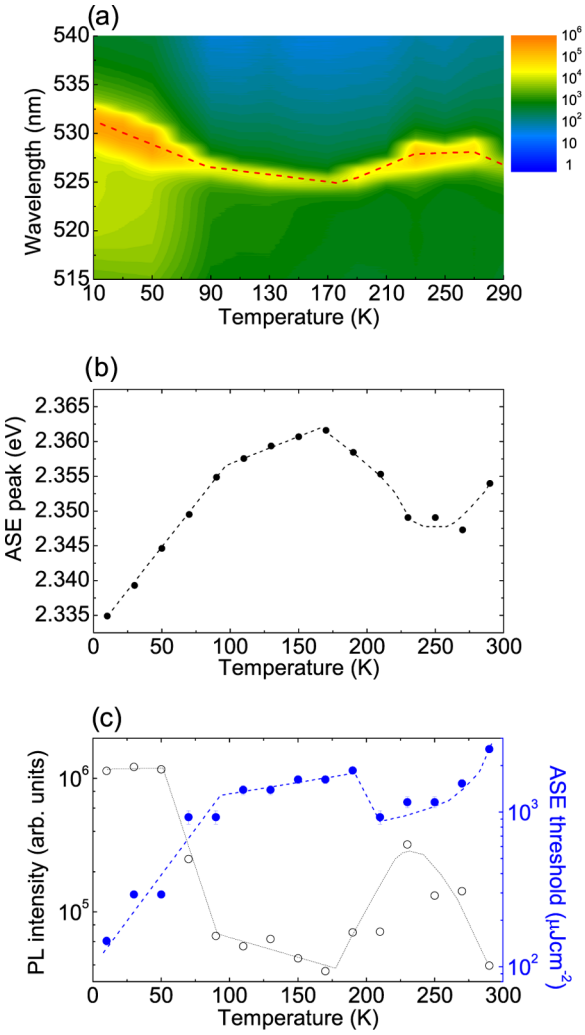

Figure 2. (a) Two-dimensional (2D) map of the PL spectra temperature dependence above the ASE threshold. The red dashed line evidences the peak wavelength position. (b) Temperature dependence of the ASE peak energy. (c) Temperature dependence of the total intensity and of the ASE threshold.

170 K is in good agreement with the one found in similar nanocrystals (NCs) in literature,[17] whereas the slope variation above 170 K has not been observed to date.

Concerning the PL intensity, we observe that previous investigations on $CsPbBr_3$ NCs allowed to observe an intensity quenching as the temperature increases, generally around 10% in NCs realized at high temperature, both in thin films[17] and in inert matrix,[16] and much higher in NCs synthesized at room temperature.[31,32] A PL intensity increase with the temperature has been instead recently observed in formamidinium lead triiodide NCs and ascribed to thermally induced exciton detrapping from surface state, whereas the same material in thin films only shows a strong quenching.[14]

The investigation of the PL spectra temperature dependence, based on a multi-Gaussian fitting (see Supporting Information), evidences that the spectra can be reproduced with the superposition of two Gaussian curves up to 170 K, whereas a third Gaussian at high wavelength is needed to reproduce the spectra at higher temperatures (see Figure S3). The presence of distinct peaks in the PL spectra of perovskites has been often reported to date and ascribed to a wide variety of processes, like

DOI: 10.1021/acs.jpcc.8b01419
J. Phys. Chem. C 2018, 122, 5813−5819

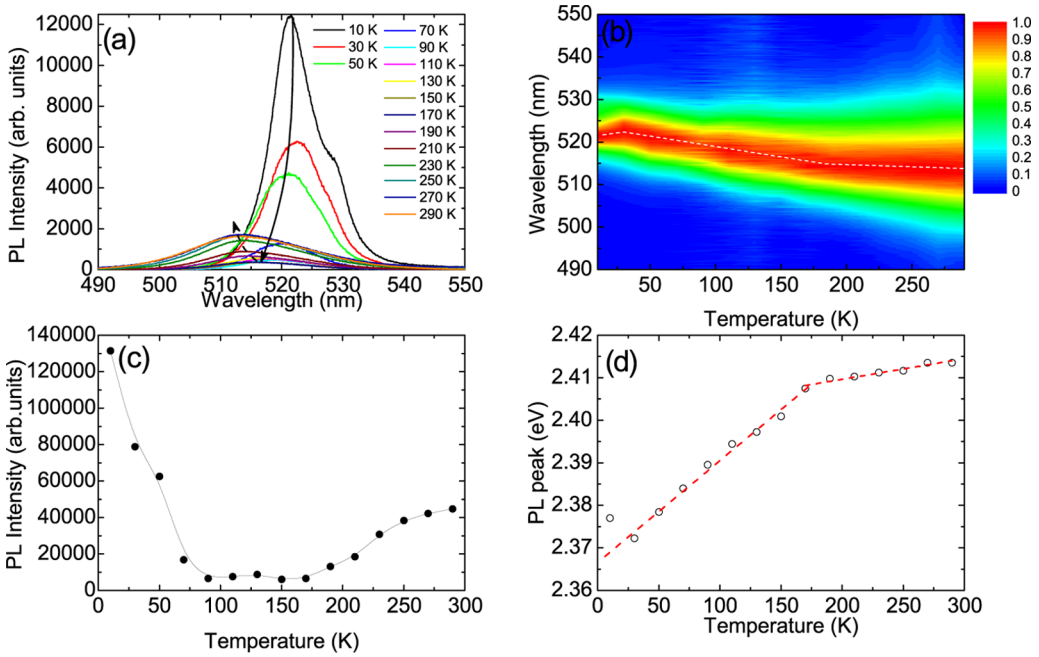

Figure 3. (a) Temperature dependence of the PL spectra temperature below the ASE threshold. (b) Two-dimensional (2D) map of the spectra (normalized to the peak value) evidencing the temperature-dependent shift of the peak wavelength (dotted line). (c) Temperature dependence of the total intensity. (d) Temperature dependence of the PL peak energy. The lines are the best fit curves of a linear fit.

the coexistence of a majority crystalline phase with inclusions of a different crystalline phase,[15,22,23,33] emission of free excitons and donor−acceptor pairs,[23] or emission of free excitons and bound excitons.[9,34] In particular, the coexistence of a narrow PL peak and a broader red-shifted peak has been observed at T = 10 K in $CsPbBr_3$ NCs films[35] and in microstructures of $FAPbBr_3$ and ascribed to the coexistence of free excitons and bound excitons emission, respectively.[34] According to this attribution, the line shape variation between 10 and 30 K could be ascribed to a variation of the peak at high energy from a narrow free exciton peak at 521 nm to a broader bound exciton peak at 524.4 nm, with an increase of the total line width and a decrease of the emission intensity. In the temperature range between 30 and 90 K, both peaks show a strong and quantitatively comparable quenching (see Figure S4), leading to a total strong PL intensity decrease but a constant relative contribution to the total intensity (see Figure S5). This behavior suggests that the two Gaussian peaks simply come from a non-Gaussian PL line shape, showing a similar temperature evolution across the emission spectral range, due to energy migration/transfer from the smaller nanocrystal to the larger ones, within the Gaussian size distribution (see Figure S1b), as also observed in $CsPbBr_3$ NCs solutions.[36] As the temperature increases, a clear blue shift of the low wavelength peak (peak 1) is observed, whereas the high wavelength peak (peak 2) shows a weak red shift (see Figure S6).

The intensity quenching in this temperature range evidences a trapping by nonshallow radiative defects that is always thermally activated.[26] A further explanation could be a temperature-induced increase of the self-absorption due to the thermal broadening of the exciton absorption peak,[19] that could produce relevant effects in the used waveguide collection geometry. In the range between 90 and 170 K, the weak total intensity decrease is due to the interplay between the intensity decrease of peak 1 (3.7 times) and a strong (7.4 times) intensity recovery of peak 2, leading to a progressive increase of the peak 2 relative contribution to the total intensity. This behavior evidences the formation of a new specie emitting in the low energy side of the spectra. Above 170 K, a further emission contribution in the low energy side of the spectrum appears, described by peak 3, accounting for about 20% of the total emission intensity with a comparable relative intensity decrease of peak 1. This new emission feature initially red-shifts up to 210 K and then blue-shifts.

This analysis thus evidences that the PL and ASE variations around 90 and 170−190 K are related to the formation of two new emitting species in the high-wavelength range of the spectra, described by a peak initially red shifting and then blue shifting.

We also observe that the intensity variations of the Gaussian peaks are strictly related to the peak wavelength temperature dependence, both of the spontaneous emission and of the ASE band (see Figure S6). In particular, both PL and ASE peaks show an identical blue shift up to 90 K, as determined by the temperature dependence of the peak wavelength of peak 1. Above 90 K, the decrease of the ASE blue-shift slope and increase of the ASE threshold take place in correspondence to the peak 2 intensity recovery, reflecting the strong dependence of the ASE band on the variation of the emission properties in the low-energy tail of the PL spectrum, where self-absorption is negligible. A remarkable correlation is also observed between the ASE peak wavelength and the peak wavelength of peak 3, above 170 K, clearly evidencing that ASE originates from the emitter at lower energy. The general intensity recovery and improvement of the ASE properties above 170 K are in apparent contrast to previous reports of PL quenching of the PL intensity of $CsPbBr_3$ NCs, both in neat films[17] and in inert polymer matrix,[16] ascribed to exciton thermal dissociation. We ascribe this effect to the interplay between emission quenching due to exciton dissociation and a dominating reduction of self-absorption due to the decrease of the exciton absorption below

DOI: 10.1021/acs.jpcc.8b01419
J. Phys. Chem. C 2018, 122, 5813−5819

the energy gap, overall leading to an increase of the intensity collected from the waveguide edge.[37]

Concerning the attribution of the temperature-induced formation of emitting states at low energy, we exclude any role of macroscopic crystalline phase transitions, as $CsPbBr_3$ is characterized, both in bulk and in NCs, by an average orthorhombic crystal structure,[38−40] whereas phase transitions toward tetragonal and cubic phases only take place above room temperature.[38] We also exclude relevant roles of trapping and detrapping processes, recently observed to affect the ASE properties of $CsPbBr_3$ bulk polycrystalline thin films[26] due to the observed complex temperature dependence of the PL line shape. Although in general a thermally activated trapping (detrapping) could lead to a temperature-dependent PL quenching (enhancement), the full explanation of our results would require a too complex interplay between trapping and detrapping processes, i.e., a trapping with a very low activation energy leading to a global PL quenching up to 90 K, followed by a simultaneous trapping-induced PL quenching at low wavelength and a detrapping at high wavelength between 90 and 170 K, and finally a general detrapping-induced PL increase above 170 K, in contrast with the PL quenching reported in previous experiments.[16,17]

The thermal activation of the increase of emission in the high-wavelength range with the simultaneous intensity decrease at short wavelength is instead qualitatively consistent with the thermal activation of energy migration/transfer from small nanocrystals (emitting at short wavelength) toward the large ones (emitting at high wavelength) within the nanocrystal size distribution (see Figure S1). In this case, at low temperature, the small available thermal energy should prevent long-range energy migration, only allowing spontaneous energy migration toward low energy (down-hill migration),[41] resulting in a temperature-independent line shape. As the temperature increases, the thermal activation of energy migration toward high-energy sites (up-hill migration) allows a long-range migration toward deeper energy minima, thus overall increasing the emission at high wavelength at the expense of the one at low wavelength. Our results are anyway not consistent with this expected dependence in many points. First of all, the low temperature data (up to 90 K) evidence the presence of two peaks with similar intensity decrease up to 90 K, compatible with the absence of thermally activated energy migration. However, this does not lead to a temperature-independent line shape as we observe a continuous broadening at high wavelength evidenced by the peak 2 red shift. A further important difference between our data and the expected behavior of thermally activated energy migration is the presence of two temperatures at which both the spontaneous emission and the ASE temperature dependences strongly change, whereas long-range energy migration typically shows a single activation energy.

Our results are instead consistent with the recent attribution of the complex X-ray spectra of $CsPbBr_3$ NCs to the presence within the NC of a nearly ordered orthorhombic subdomains, separated by a network of twin boundaries, with a number increasing with the temperature.[40] Similar conclusions have been also recently obtained to explain the presence of multipeak PL spectra in polycrystalline solution processes perovskites thin films, attributing the subdomains to different order level of the organic component.[21] The presence of two clear transition temperatures between the different observed emission regimes, namely, 90 and 170 K, suggests that the twin boundaries formation requires specific value of the lattice parameters that are temperature-dependent due to the thermal expansion. Moreover, the temperature dependence of the peak wavelength of peak 2 up to 110 K, and of peak 3 and of the ASE peak above 170 K, showing a red shift followed by a blue shift, is consistent with an initial temperature-induced increase of the subdomains dimensions followed by a dominant contribution of the lattice expansion-induced blue shift. The formation of these disordered domains results in the increase of the emission at low energy[21] and clearly modifies the PL spectra, strongly affecting the ASE properties.

CONCLUSIONS

In conclusion, we investigated the temperature dependence of the spontaneous and stimulated emissions of $CsPbBr_3$ NCs in thin films, evidencing the presence of three different emission regimes, ascribed to the formation and the temperature evolution of partially disordered subdomains, strongly affecting the macroscopic ASE properties of the films. Our results improve the understanding of the perovskite NCs light amplification properties demonstrating that the total ASE properties of NCs thin films are mainly determined by the emission properties of a minority distribution of subdomains emitting at low energy.

ASSOCIATED CONTENT

Supporting Information

The Supporting Information is available free of charge on the ACS Publications website at DOI: 10.1021/acs.jpcc.8b01419.

Nanocrystals materials and synthesis details; TEM characterization of the shape and the size of the NCs (Figure S1); PLQY in solution; SEM and fluorescence microscopy of the film morphology (Figure S2); details of the multi-Gaussian fitting; temperature dependence of the number of Gaussian peaks (Figure S3); temperature dependence of the peaks intensity (Figure S4), relative intensity (Figure S5) and peak wavelength (Figure S6) (PDF)

AUTHOR INFORMATION

Corresponding Author

*E-mail: marco.anni@unisalento.it. Phone: +39 0832 297540.

ORCID

Maria Luisa De Giorgi: 0000-0002-3774-6477

Maksym V. Kovalenko: 0000-0002-6396-8938

Marco Anni: 0000-0002-1651-0166

Notes

The authors declare no competing financial interest.

ACKNOWLEDGMENTS

M.K. acknowledges financial support from the European Union through the FP7 (ERC Starting Grant NANOSOLID, GA No. 306733).

REFERENCES

(1) National Renewable Energy Laboratory. Research Cell Record Efficiency Chart. https://www.nrel.gov/pv/assets/images/efficiency-chart.png (accessed July 4, 2017).

(2) Edri, E.; Kirmayer, S.; Mukhopadhyay, S.; Gartsman, K.; Hodes, G.; Cahen, D. Elucidating the Charge Carrier Separation and Working Mechanism of CH3NH3PbI3-xClx Perovskite Solar Cells. *Nat. Commun.* **2014**, *5*, No. 3461.

DOI: 10.1021/acs.jpcc.8b01419
J. Phys. Chem. C 2018, 122, 5813−5819

(3) Shi, D.; Adinolfi, V.; Comin, R.; Yuan, M.; Alarousu, E.; Buin, A.; Chen, Y.; Hoogland, S.; Rothenberger, A.; Katsiev, K.; et al. Low Trap-State Density and Long Carrier Diffusion in Organolead Trihalide Perovskite Single Crystals. *Science* **2015**, *347*, 519−522.
(4) Protesescu, L.; Yakunin, S.; Bodnarchuk, M. I.; Krieg, F.; Caputo, R.; Hendon, C. H.; Yang, R. X.; Walsh, A.; Kovalenko, M. V. Nanocrystals of Cesium Lead Halide Perovskites (CsPbX3, X = Cl, Br, and I): Novel Optoelectronic Materials Showing Bright Emission with Wide Color Gamut. *Nano Lett.* **2015**, *15*, 3692−3696.
(5) Noh, J. H.; Im, S. H.; Heo, J. H.; Mandal, T. N.; Seok, S. I. Chemical Management for Colorful, Efficient, and Stable Inorganic Organic Hybrid Nanostructured Solar Cells. *Nano Lett.* **2013**, *13*, 1764−1769.
(6) Protesescu, L.; Yakunin, S.; Kumar, S.; Bär, J.; Bertolotti, F.; Masciocchi, N.; Guagliardi, A.; Grotevent, M.; Shorubalko, I.; Bodnarchuk, M. I.; et al. Dismantling the "Red Wall" of Colloidal Perovskites: Highly Luminescent Formamidinium and Formamidinium-Cesium Lead Iodide Nanocrystals. *ACS Nano* **2017**, *11*, 3119−3134.
(7) Nedelcu, G.; Protesescu, L.; Yakunin, S.; Bodnarchuk, M. I.; Grotevent, M. J.; Kovalenko, M. V. Fast Anion-Exchange in Highly Luminescent Nanocrystals of Cesium Lead Halide Perovskites (CsPbX3, X = Cl, Br, I). *Nano Lett.* **2015**, *15*, 5635−5640.
(8) Akkerman, Q. A.; D'Innocenzo, V.; Accornero, S.; Scarpellini, A.; Petrozza, A.; Prato, M.; Manna, L. Tuning the Optical Properties of Cesium Lead Halide Perovskite Nanocrystals by Anion Exchange Reactions. *J. Am. Chem. Soc.* **2015**, *137*, 10276−10281.
(9) Xing, G.; Nripan, M.; Lim, S. S.; Yantara, N.; Liu, X.; Sabba, D.; Grätzel, M.; Mhaisalkar, S.; Sum, T. C. Low-Temperature Solution-Processed Wavelength-Tunable Perovskites for Lasing. *Nat. Mater.* **2014**, *13*, 476−480.
(10) Yakunin, S.; Protesescu, L.; Krieg, F.; Bodnarchuk, I.; Maryna; Nedelcu, G.; Humer, M.; De Luca, G.; Fiebig, M.; Heiss, W.; Kovalenko, M. V. Low-Threshold Amplified Spontaneous Emission and Lasing From Colloidal Nanocrystals of Caesium Lead Halide Perovskites. *Nat. Commun.* **2015**, *6*, No. 8056.
(11) Deschler, F.; Price, M.; Pathak, S.; Klintberg, L. E.; Jarausch, D.-D.; Higler, R.; Hüttner, S.; Leijtens, T.; Stranks, S. D.; Snaith, H. J.; et al. High Photoluminescence Efficiency and Optically Pumped Lasing in Solution-Processed Mixed Halide Perovskite Semiconductors. *J. Phys. Chem. Lett.* **2014**, *5*, 1421−1426.
(12) Dhanker, R.; Brigeman, A. N.; Larsen, A. V.; Stewart, R. J.; Asbury, J. B.; Giebink, N. C. Random Lasing in Organo-Lead Halide Perovskite Microcrystal Networks. *Appl. Phys. Lett.* **2014**, *105*, No. 151112.
(13) Whitworth, G. L.; Harwell, J. R.; Miller, D. N.; Hedley, G. J.; Zhang, W.; Snaith, H. J.; Turnbull, G. A.; Samuel, I. D. W. Nanoimprinted Distributed Feedback Lasers of Solution Processed Hybrid Perovskites. *Opt. Express* **2016**, *24*, 23677−23684.
(14) Fang, H.-H.; Protesescu, L.; Balazs, D. M.; Adjokatse, S.; Kovalenko, M. V.; Loi, M. A. Exciton Recombination in Formamidinium Lead Triiodide: Nanocrystals versus Thin Films. *Small* **2017**, *13*, No. 1700673.
(15) Wu, K.; Bera, A.; Ma, C.; Du, Y.; Yang, Y.; Li, L.; Wu, T. Temperature-Dependent Excitonic Photoluminescence of Hybrid Organometal Halide Perovskite Films. *Phys. Chem. Chem. Phys.* **2014**, *16*, 22476−22481.
(16) Diroll, B. T.; Nedelcu, G.; Kovalenko, M. V.; Schaller, R. D. High-Temperature Photoluminescence of CsPbX3 (X = Cl, Br, I) Nanocrystals. *Adv. Funct. Mater.* **2017**, *27*, No. 1606750.
(17) Li, J.; Yuan, X.; Jing, P.; Li, J.; Wei, M.; Hua, J.; Zhao, J.; Tian, L. Temperature-Dependent Photoluminescence of Inorganic Perovskite Nanocrystal Films. *RSC Adv.* **2016**, *6*, 78311−78316.
(18) Sestu, N.; Cadelano, M.; Sarritzu, V.; Chen, F.; Marongiu, D.; Piras, R.; Mainas, M.; Quochi, F.; Saba, M.; Mura, A.; et al. Absorption F-Sum Rule for the Exciton Binding Energy in Methylammonium Lead Halide Perovskites. *J. Phys. Chem. Lett.* **2015**, *6*, 4566−4572.
(19) D' Innocenzo, V.; Grancini, G.; Alcocer, M. J. P.; Kandada, A. R. S.; Stranks, S. D.; Lee, M. M.; Lanzani, G.; Snaith, H. J.; Petrozza, A. Excitons Versus Free Charges in Organo-Lead Tri-Halide Perovskites. *Nat. Commun.* **2014**, *5*, No. 3586.
(20) Li, D.; Wang, G.; Cheng, H.-C.; Chen, C.-Y.; Wu, H.; Liu, Y.; Huang, Y.; Duan, X. Size-Dependent Phase Transition in Methylammonium Lead Iodide Perovskite Microplate Crystals. *Nat. Commun.* **2016**, *7*, No. 11330.
(21) Dar, M. I.; Jacopin, G.; Meloni, S.; Mattoni, A.; Arora, N.; Boziki, A.; Zakeeruddin, S. M.; Rothlisberger, U.; Grätzel, M. Origin of Unusual Bandgap Shift and Dual Emission in Organic-Inorganic Lead Halide Perovskites. *Sci. Adv.* **2016**, *2*, No. e1601156.
(22) Wehrenfennig, C.; Liu, M.; Snaith, H. J.; Johnston, M. B.; Herz, L. M. Charge Carrier Recombination Channels in the Low-Temperature Phase of Organic-Inorganic Lead Halide Perovskite Thin Films. *APL Mater.* **2014**, *2*, No. 081513.
(23) Kong, W.; Ye, Z.; Qi, Z.; Zhang, B.; Wang, M.; Rahimi-Iman, A.; Wu, H. Characterization of an Abnormal Photoluminescence Behavior Upon Crystal-Phase Transition of Perovskite CH3NH3PbI3. *Phys. Chem. Chem. Phys.* **2015**, *17*, 16405−16411.
(24) Kao, T. S.; Chou, Y.-H.; Chou, C.-H.; Chen, F.-C.; Lu, T.-C. Lasing Behaviors upon Phase Transition in Solution-Processed Perovskite Thin Films. *Appl. Phys. Lett.* **2014**, *105*, No. 231108.
(25) Qin, L.; Lv, L.; Li, C.; Zhu, L.; Cui, Q.; Hu, Y.; Lou, Z.; Teng, F.; Hou, Y. Temperature Dependent Amplified Spontaneous Emission of Vacuum Annealed Perovskite Films. *RSC Adv.* **2017**, *7*, 15911−15916.
(26) De Giorgi, M. L.; Perulli, A.; Yantara, N.; Boix, P. P.; Anni, M. Amplified Spontaneous Emission Properties of Solution Processed CsPbBr3 Perovskite Thin Films. *J. Phys. Chem. C* **2017**, *121*, 14772−14778.
(27) Brouwer, A. M. Standards for Photoluminescence Quantum Yield Measurements in Solution (IUPAC Technical Report). *Pure Appl. Chem.* **2011**, *83*, 2213−2228.
(28) Becker, M.; Fan, H. Y. Optical Properties of Semiconductors. III. Infra-Red Transmission of Silicon. *Phys. Rev.* **1949**, *76*, 1531−1532.
(29) Bardeen, J.; Shockley, W. Deformation Potentials and Mobilities in Non-Polar Crystals. *Phys. Rev.* **1950**, *80*, 72−80.
(30) Fan, H. Y. Temperature Dependence of the Energy Gap in Monatomic Semiconductors. *Phys. Rev.* **1950**, *78*, 808−809.
(31) Li, X.; Wu, Y.; Zhang, S.; Cai, B.; Gu, Y.; Song, J.; Zeng, H. CsPbX3 Quantum Dots for Lighting and Displays: Room-Temperature Synthesis, Photoluminescence Superiorities, Underlying Origins and White Light-Emitting Diodes. *Adv. Funct. Mater.* **2016**, *26*, 2435−2445.
(32) Wei, S.; Yang, Y.; Kang, X.; Wang, L.; Huang, L.; Pan, D. Room-Temperature and Gram-Scale Synthesis of CsPbX3 (X = Cl, Br, I) Perovskite Nanocrystals with 50-85% Photoluminescence Quantum Yields. *Chem. Commun.* **2016**, *52*, 7265−7268.
(33) Diab, H.; Trippé-Allard, G.; Lédée, F.; Jemli, K.; Vilar, C.; Bouchez, G.; Jacques, V. L.; Tejeda, A.; Even, J.; Lauret, J.-S.; et al. Narrow Linewidth Excitonic Emission in Organic Inorganic Lead Iodide Perovskite Single Crystals. *J. Phys. Chem. Lett.* **2016**, *7*, 5093−5100.
(34) Dai, J.; Zheng, H.; Zhu, C.; Lu, J.; Xu, C. Comparative Investigation on Temperature-Dependent Photoluminescence of CH3NH3PbBr3 and CH(NH2)2PbBr3 Microstructures. *J. Mater. Chem. C* **2016**, *4*, 4408−4413.
(35) Lee, S. M.; Moon, C. J.; Lim, H.; Lee, Y.; Choi, M. Y.; Bang, J. Temperature-Dependent Photoluminescence of Cesium Lead Halide Perovskite Quantum Dots: Splitting of the Photoluminescence Peaks of CsPbBr3 and CsPb(Br/I)3 Quantum Dots at Low Temperature. *J. Phys. Chem. C* **2017**, *121*, 26054−26062.
(36) de Weerd, C.; Navascues, L.; Zhang, H.; Buma, W.; Nedelcu, G.; Kovalenko, M.; Gregorkiewicz, T. Energy Transfer Between Inorganic Perovskite Nanocrystals. *J. Phys. Chem. C* **2016**, *120*, 13310−13315.
(37) Anni, M. Photodegradation Effects on the Emission Properties of an Amplifying Poly(9,9-dioctylfluorene) Active Waveguide Operating in Air. *J. Phys. Chem. B* **2012**, *116*, 4655−4660.

DOI: 10.1021/acs.jpcc.8b01419
J. Phys. Chem. C 2018, 122, 5813−5819

(38) Rodová, M.; Brozek, J.; Knízek, K.; Nitsch, K. Phase Transitions in Ternary Caesium Lead Bromide. *J. Therm. Anal. Calorim.* **2003**, *71*, 667−673.
(39) Cottingham, P.; Brutchey, R. L. On the Crystal Structure of Colloidally Prepared CsPbBr3 Quantum Dots. *Chem. Commun.* **2016**, *52*, 5246−5249.
(40) Bertolotti, F.; Protesescu, L.; Kovalenko, M. V.; Yakunin, S.; Cervellino, A.; Billinge, S. J. L.; Terban, M. W.; Pedersen, J. S.; Masciocchi, N.; Guagliardi, A. Coherent Nanotwins and Dynamic Disorder in Cesium Lead Halide Perovskite Nanocrystals. *ACS Nano* **2017**, *11*, 3819−3831.
(41) Meskers, S. C. J.; Hübner, J.; Oestreich, M.; Bässler, H. Dispersive Relaxation Dynamics of Photoexcitations in a Polyfluorene Film Involving Energy Transfer: Experiment and Monte Carlo Simulations. *J. Phys. Chem. B* **2001**, *105*, 9139−9149.

DOI: 10.1021/acs.jpcc.8b01419
J. Phys. Chem. C 2018, 122, 5813−5819